Journal of Applied Fluid Mechanics, Vol. 18, No. 9, pp. 2332-2348, 2025.
Available online at www.jafmonline.net, ISSN 1735-3572, EISSN 1735-3645.
https://doi.org/10.47176/jafm.18.9.3328

Computational Fluid Dynamics Study on the Aerodynamics of a Blended Wing Body with Ground Effect in Subsonic Conditions

S. Mohan† and P. Kumar

Department of Space Engineering and Rocketry, Mesra, Ranchi, 813210, Jharkhand, India

†*Corresponding Author Email: phdser10001@bitmesra.ac.in*

ABSTRACT

Blended Wing Body (BWB) aircraft designs have garnered significant interest due to their potential for improved aerodynamic efficiency, particularly during critical phases of flight such as landing and take-off. This study was conducted to analyse the aerodynamic performance of BWB aircraft during ground effect interactions, which are crucial for understanding performance in these phases. Numerical simulations have been performed at a free-stream velocity of 18m/s. A moving ground velocity of 18 m/s has been imparted to avoid the formation of the boundary layer on the ground. Simulations were conducted at a Reynolds number of 85,525 based on MAC, with angles of attack ranging from -10 to 30 degrees and ground heights normalized by wingspan (h/b) between 0.2 and 1. The effect of the angle of attack and ground heights has been investigated. The investigations aim to capture the complex flow behaviour due to the varying ground proximities. The results at extremely close proximity revealed noticeable disparities in the normalised velocity and pressure distributions in the leeward location, highlighting the significant impact of the ground effect on aerodynamic performance. These findings contribute to a comprehensive understanding and analysis of BWB aircraft behaviour during ground proximity operations, providing insights for optimising proximities and improving safety and efficiency during landing and take-off.

Article History

Received December 19, 2024
Revised March 16, 2025
Accepted April 24, 2025
Available online July 5, 2025

Keywords:

Ground effect
Pitching
Pressure distribution
Blended wing body
Lift
Drag

1. INTRODUCTION

The Blended Wing Body (BWB) aircraft concept represents an innovation in modern aerodynamics, which has offered improvements in efficiency and performance over conventional tube-and-wing configurations of aircrafts. Boeing in 1993 conceptualized the BWB project that aimed to develop midsize (BWB-250) and large (BWB-450) transport aircraft for both military and commercial applications. The primary objective of these designs is to achieve a balance between high aerodynamic efficiency and safety standards comparable to established aircraft such as the Boeing 777. A fundamental challenge in this endeavor is creating an airframe that simultaneously satisfies the diverse requirements of military and commercial stakeholders. A successful resolution to this challenge could pave the way for revolutionary advancements in aircraft design and development (Liebeck, 2003).

One of the key advantages of the BWB configuration is its potential for substantial reductions in fuel consumption and takeoff weight. Comparative studies have demonstrated that an 800-passenger BWB aircraft could achieve a 15% reduction in takeoff weight and a 27% decrease in fuel consumption per seat mile compared to conventional designs. These efficiency gains have led to the development of BWB aircraft for passenger capacities ranging from 200 to 600, with an emphasis on part commonality and manufacturing efficiency (Liebeck, 2004). Furthermore, recent aerodynamic analyses indicate that the BWB can operate at cruise Mach numbers up to 0.95, exceeding earlier performance expectations.

Despite its promising benefits, the BWB configuration presents unique aerodynamic challenges, particularly in low-speed flight regimes such as takeoff and landing. The aerodynamic properties of such an aircraft differ significantly from those of traditional configurations due to its unconventional lifting body design, large sweepback, washout, and reflex wing configurations. Figure 1 depicts a typical flow field over a Blended Wing Body (BWB). A lot of research has been conducted on an optimized BWB configurations dealing with fundamental aerodynamic principles, including lift, drag, airfoil design, and flow separation, providing

NOMENCLATURE

U_∞	free stream velocity	x/c	non-dimensional chord-wise location along stream-wise direction
$\Gamma/U_\infty c$	normalized circulation	y/s	non-dimensional wing spanwise location along stream-wise direction
Re	Reynolds number based on the MAC	h/c	ratio between height above BWB and mean chord length
C_L	lift coefficient (=L/ (q_∞S))	AoA	Angle of Attack
C_D	drag coefficient (=D/ (q_∞S))	x_{cg}	leading edge to center of gravity
C_M	pitching moment coefficient (=PM/ (q∞Sc)) (pitching moment negative for nose down)	x_{ac}	leading edge to aerodynamic center
x_{ac}	leading edge to aerodynamic center		

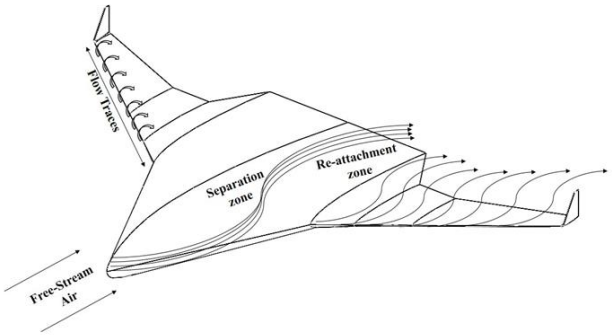

Fig. 1 Flow field distribution around BWB

valuable insights into the configuration (Gudmundsson, 2014). Moreover, various experimental and computational studies conducted in the past have investigated the aerodynamic behavior of BWB configurations under different conditions. Qin et al. (2004) explored the aerodynamic characteristics of BWB aircraft using viscous flow simulations which demonstrated improvements in aerodynamic efficiency through inverse twist design. Similarly, Kashitani et al. (2015) conducted wake measurement investigations on a BWB model at a free-stream velocity of 25 m/s, revealing that both the wings and center body contribute to lift, while induced drag peaks occur at angles of attack of 8 deg and 10 deg. Other studies, such as those by Yamada et al. (2019) and Min et al. (2008), have investigated stability and autopilot mechanisms for BWB UAV configurations.

While the past research has provided valuable insights into the aerodynamic performance of BWB configuration, a critical aspect that remains largely unexplored is the influence of ground proximity on the flow behavior of BWB configuration which is experienced during the take-off and landing conditions. Ground effect is the phenomenon where an aircraft experiences increased lift and reduced drag when flying near the ground. This phenomenon is well-documented for conventional aircraft/ wings. How (2024) demonstrated an optimization methodology for wing-in-ground (WIG) effect aircraft, improving lift-to-drag ratios and static height stability. Similar studies by Schweikhard (1967) and Lee et al. (1989) have investigated the influence of ground proximity on different wing configurations, including delta wings and high-speed aircraft such as the F-106B and XB-70. However, numerical simulations of ground effect remain a challenge, as noted by Barber et al. (1999), who proposed the use of moving ground conditions in computational analyses. Zhang and Zerihan (2003) further explored the off-surface aerodynamic characteristics of wings in ground effect, finding that wake expansion and vortex breakdown influence aerodynamic forces.

Experimental and computational investigations into the impact of ground effect on airfoil and wing configurations have provided valuable findings. Ahmed and Sharma (2005) analyzed the flow characteristics of a NACA 0015 airfoil in ground effect, showing that ground proximity raises the pressure coefficient on the lower surface, enhancing lift. However, at higher angles of attack, adverse pressure gradients intensify wake turbulence, leading to increased drag. Rozhdestvensky (2006) reviewed the research and development of WIG technology, covering aerodynamic modeling, stability, and structural considerations. Subsequent numerical studies have further explored ground effect phenomena in various wing configurations. For instance, Angle et al. (2009) examined the influence of slots on airfoils in ground effect, revealing that optimized slot configurations can stabilize center-of-pressure movement and improve pitch stability. Molina and Zhang (2011) showed different aerodynamic regimes for inverted airfoils undergoing heaving motion near the ground Qu et al. (2015) examined the influence of ground proximity on delta wings, highlighting variations in lift, drag, and vortex behavior across different angles of attack. Tumse et al. (2021) further examined the effects of ground proximity on delta wings with a 40° sweep angle, noting improved lift-to-drag ratios and modifications in vortex dynamics at reduced ground clearance.

Although extensive research has explored ground effect on various wing and airfoil configurations, studies focused on the aerodynamic behavior of BWB aircraft in ground effect remain limited. It is a well-known fact that the BWB configuration significantly differs from conventional aircraft. Hence understanding its aerodynamic characteristics during take-off and landing is crucial for better design and stability. The distinct lifting body design of the BWB configuration shows how aerodynamic forces are distributed in ground effect. This calls for the need to fill this gap in existing literature adopting experiments and computations.

The present research aims to investigate the impact of ground effect on BWB aircraft at different angles of attack, focusing on varying ground clearances during take-

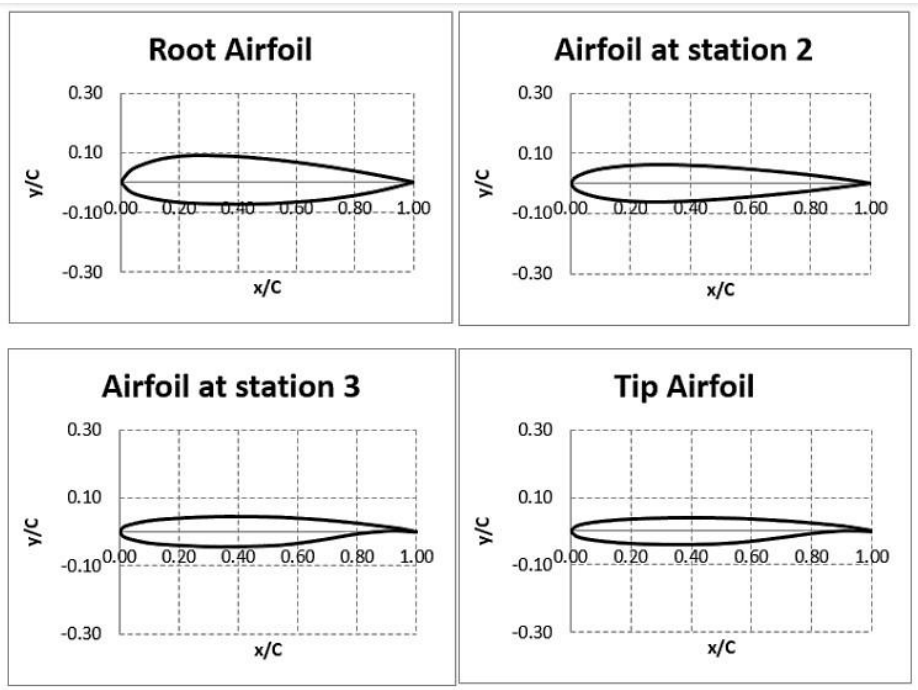

Fig. 2 Schematic representation of section-wise aerofoil profiles and dimensions of BWB (dimensions in mm)

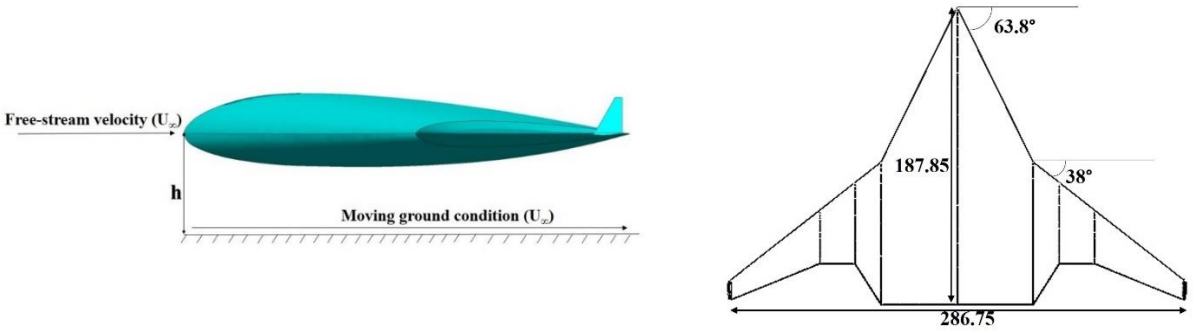

(b)

Fig. 3 Schematic representation of ground effect over BWB

off and landing. Computational techniques have been adopted on the BWB model using commercially available computational fluid dynamics (CFD) software, FLUENT. The objective is to explore the underlying aerodynamic principles governing BWB aircraft behavior in ground proximity, ultimately contributing to improved aircraft design and operational efficiency. Addressing this knowledge gap is essential for better BWB technology, particularly for designing a high-efficiency, next-generation aircraft.

2. METHODOLOGY OF COMPUTATIONAL SETUP

The present study involved comprehensive numerical simulations over a conventional BWB configuration, as depicted in Fig. 2, which is similar to the one reported by Qin et al. (2004). Figure 3 demonstrates the setup configuration for the ground effect on the BWB utilised in the present study. The study conducted unsteady computational simulations on a BWB configuration to investigate its external aerodynamics under a free-stream velocity of 18 m/s. The computational analysis utilized commercial software FLUENT, which is adept at numerically solving the unsteady Reynolds Averaged Navier-Stokes (uRANS) equations. The study employed hybrid grid development for the domain and BWB model. This involved using a structured BWB surface mesh and an unstructured volume mesh, with particular emphasis on refining the surface grids near the body and ground to ensure an accurate representation of the flow field. The computational surface mesh was rotated to specified angles to change the angle of attack on the BWB. Hence,

Special focus was given to areas exposed to different attack angles, where the grids were made denser to capture the complexities of wake flow better. The initial cell distance from the surface remained at 3×10^{-4} times the chord length, optimizing the mesh to capture detailed flow characteristics to maintain computational efficiency. The mesh near ground proximity was also refined to better approximate boundary layer effects and ground interaction. Additionally, special care was taken to ensure the mesh transitioned smoothly between different refinement levels to avoid numerical inaccuracies near the surface. Overall, the detailed meshing strategy proved crucial in accurately simulating the flow behaviour in challenging areas of geometry. Specific boundary conditions

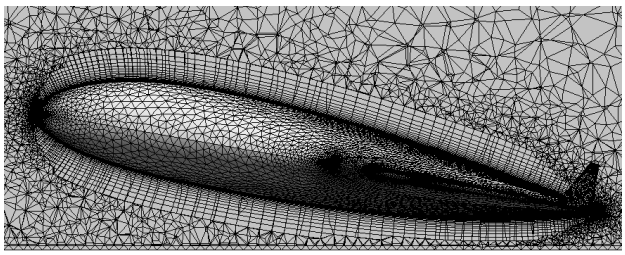

Fig. 4 Side view of grid development over BWB and in Y-Z plane

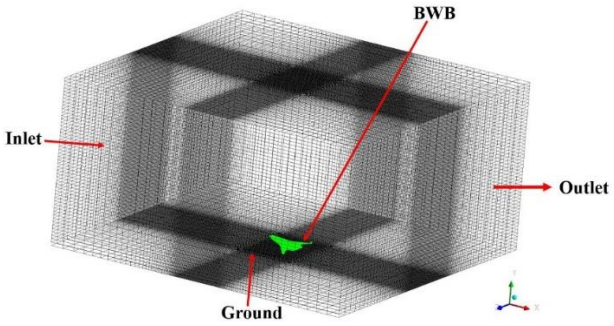

Fig. 5 Computational domain of the BWB aircraft

were applied to simulate the flow dynamics around the BWB. These included a velocity inlet condition to replicate the incoming airflow, a no-slip condition on the body surface to represent the viscous boundary layer, and an outflow condition at the domain exit to allow the simulated airflow to exit the computational domain seamlessly. Additionally, moving ground conditions equal to free-stream conditions were provided.

The computation utilized a rectangular domain and a locally refined cuboidal region to enhance computational approximation. This approach minimized computational residuals and improved the accuracy of the simulation results. Adjustments were made to the mesh refinement as the ground proximity changed, ensuring a uniform number of elements in each volume mesh. Figure 4 illustrates the grid configuration and spatial distribution across various planes, offering a detailed visualization of the computational setup. This representation ensures an accurate depiction of the flow physics around the BWB configuration. Additionally, the figure provides insight into the BWB's orientation when rotated at a specific angle. Figure 5 shows the computational domain. Residuals of mass, momentum and forces were monitored to ensure a converged solution.

Table 1 presents the results of a grid independence study on the BWB at an angle of attack (α) of 0 degrees for free-stream conditions, comparing different computational volume elements. The study demonstrated that higher grid densities exhibited closer alignment with experimental values, thereby indicating a reduction in numerical discrepancies as mesh resolution increased (Widiawaty et al., 2024). This finding suggests that, for computational studies focusing on the aerodynamic performance of BWBs, the employment of finer meshes could yield more accurate predictions, particularly in

Table 1 Grid Independence Test

α = 0°	C_L	C_D
1.5 million	0.054	0.033
2 million	0.054	0.029
3 million	0.056	0.030

Table 2 Domain Independence Test

Current Computation		
	Square Domain	Bullet Domain
C_L	0.84	0.84
C_D	0.11	0.11

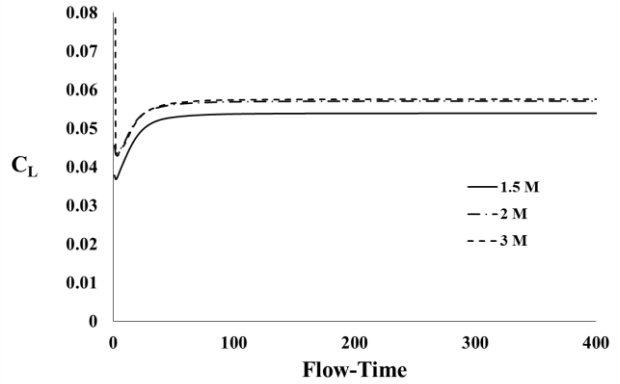

Fig. 6 Time history of lift coefficient for three meshes

critical areas such as aerodynamic coefficients and flow separation points. Nonetheless, balancing the requirement for higher grid densities with computational resource constraints is essential, ensuring that the selected mesh resolution represents a practical compromise between accuracy and computational efficiency. For this investigation, further computational work was conducted using a mesh with 3 million elemental cells, as this resolution more effectively captured ground proximity effects, which will be discussed in subsequent sections. The grid independence test, as well as the domain independence test, was conducted to ensure that the numerical results were not influenced by grid resolution or domain size. Multiple grid resolutions were tested, and key aerodynamic parameters were monitored to confirm convergence as shown in Table 1 below. Similarly, the domain size was varied to assess its impact on flow characteristics, ensuring that boundary interactions did not affect the results, shown in Table 2. These tests confirmed that the chosen computational setup provided accurate and reliable predictions. The time history of all three meshes provided in Table 1 are shown in Fig. 6.

This study employed the Spalart-Allmaras turbulence model, a one-equation model introduced by Spalart, and Allmaras (1992) to model the flow characteristics. This model has been identified as particularly effective for external flow simulations, as Gebbie et al. (2007) corroborated. For the computational aspects, the Green-Gauss cell-based method was utilised. A second-order discretization scheme was implemented for both spatial

and temporal terms to ensure precision in the simulation. Furthermore, the SIMPLEC algorithm was selected for the pressure-velocity coupling in the computations. The turbulence terms were also discretized using a second-order scheme to maintain consistency and accuracy in the modelling approach. The time history of all three meshes provided in table 1 are shown in figure 6.

3. RESULTS AND DISCUSSION

The subsequent sections delve into a comprehensive investigation of the aerodynamic effects experienced by BWB aircraft. By thoroughly understanding the below-mentioned interactions, the study aimed to enhance aviation safety and aircraft performance under various ground proximities. The analysis began with an examination of the free-stream conditions, focusing on how different angles of attack influenced the lift and drag coefficients. A comparison of experimental data with the results reported by Yamada et al. (2015) provides a basis for validation and identifying any discrepancies that arose from varying experimental setups. Following this, the investigation moved to the ground effect analysis, which played a crucial role in the aircraft's performance during low-altitude operations, particularly during take-off and landing. This section explored the proximity to the ground altered aerodynamic characteristics, affecting the aerodynamic and overall efficiency of the aircraft.

3.1 Free-Stream Effects

Computational analyses were performed on a representative BWB configuration, with validation conducted by comparing the results against experimental data previously reported by Yamada et al. (2019). Figure 7 presents the variation of the coefficient of lift (C_L) across different angles of attack, where a strong correlation was observed with the C_L values reported by Yamada et al. (2019). The BWB's streamlined, continuous surface, which enhances airfoil performance and optimizes boundary layer control, enabled the airflow to remain attached over a more extensive portion of the wing at varying angles of attack. This delayed onset of flow separation contributed to a more gradual stall behaviour, effectively explaining the increased lift observed in both computational and experimental results.

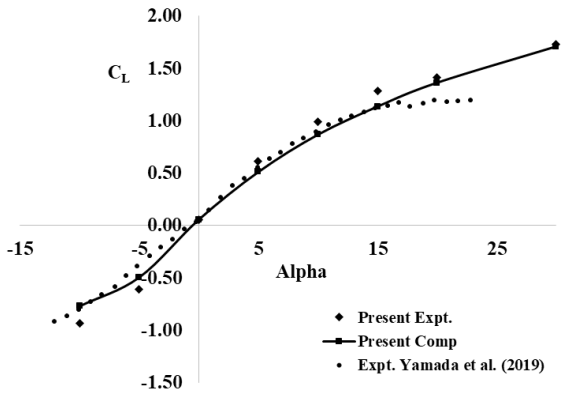

Fig. 7 C_L vs Alpha at different α

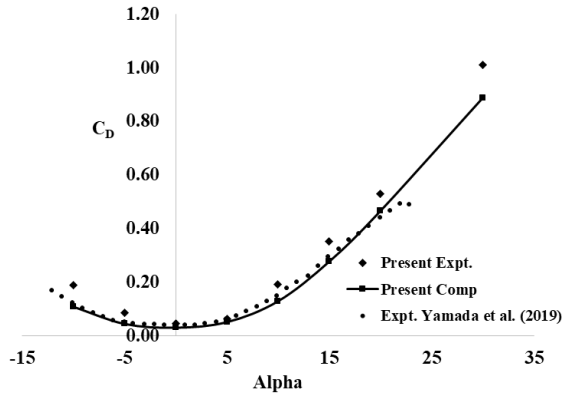

Fig. 8 C_D vs Alpha at different α

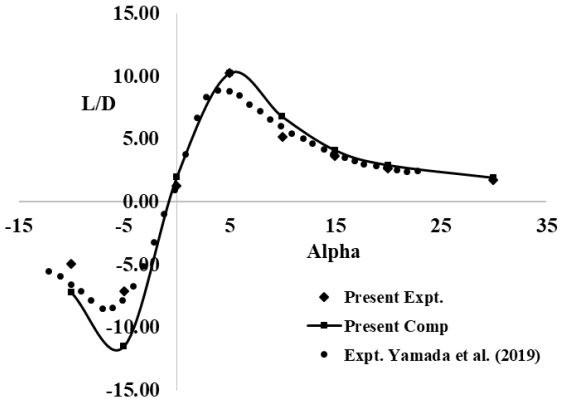

Fig. 9 L/D vs Alpha at different α

The graph in Fig. 8 illustrates the change in the drag coefficient as the angle of attack increases. It was observed that the drag increases when the angle of attack changes within positive and negative angles; the shift from laminar to turbulent flow at specific angles adds to the drag increase. This explains the parabolic trend in the drag coefficient as the angles of attack increase. The study findings closely align with the experiments conducted by Yamada et al. (2019), although there may be slight variations due to differences in model and wind tunnel conditions.

Figure 9 illustrates the impact of the angle of attack on the L/D. The maximum L/D was observed at α = 5 degrees, while the minimum was at α = -5°. There was good agreement between the computed and measured values at positive angles, but they did not align well at negative angles of attack. This discrepancy might be attributed to the more clustered grid in the upper wake compared to the lower wake at negative angles of attack. Based on the above validation in free-stream conditions, the ground effect computations were carried out to further analyse the aerodynamic performance of the aircraft during take-off and landing.

3.2 Ground Effects

As mentioned in the introduction section, the moving ground effect on BWB is quite useful for various purposes; optimising the moving ground effect is essential

not only for understanding the movement of aircraft during a turn but also for dealing with adverse conditions such as weather effects or control surface malfunctions. A thorough understanding of the ground effect can significantly improve aviation safety and optimise aircraft performance. In ground effect conditions, lift inversely correlates with free-stream scenarios. The angle of attack significantly influences the aerodynamic behaviour of an aircraft near the ground (α), which describes the angle between the oncoming air or relative wind and a reference line on the airplane or wing. As seen in Figure 10, when BWB is near the ground, specifically within a height equivalent to the wingspan or less, the ground effect comes into play, affecting both lift and drag characteristics (Fig. 11). At a (α= 0°), the presence of the ground disrupts the airflow patterns around the aircraft. This disruption increases the aerodynamic drag, the force opposing the aircraft's forward motion due to the interference of airflow beneath the wing and ground, creating a cushioning effect but also presenting additional friction.

Simultaneously, the lift force that counteracts the weight of the aircraft and enables it to remain airborne is diminished as the ground interferes with the wing's ability to generate a strong vortex and the optimal pressure difference above and below the wing. As the BWB moves away from the ground or the angle of attack changes, the influence of the ground effect diminishes. This reduction in ground effect results in an increase in the lift generated by the wings. The wing's C_L, representing lift per unit wing area at a given angle of attack, exhibits distinct behavior near the ground. At higher angles of attack, the lift-enhancing effect of ground proximity weakens, causing C_L to decrease compared to its free-stream value. Conversely, at lower angles of attack or as the aircraft descends with α close to 0°, C_L can increase due to the stabilizing and lift-enhancing influence of ground effect. This results in greater lift and potentially reduced drag compared to flying at the same angle of attack at a higher altitude (Boschetti, et al. 2022). Understanding the interplay between angle of attack, ground effect, and their impact on lift and drag is particularly important during takeoff and landing, where ground proximity significantly influences aircraft performance.

When examining the stable pitching moment within the ground effect zone, it is crucial to understand the impact of ground proximity on C_M trough alterations in the aerodynamic pressure distribution across the aircraft's surfaces.The ground effect leads to an enhancement in lift generated with a corresponding decrease in induced drag due to the interference of the ground with the airflow patterns around the aircraft. As the aircraft's CG approaches the ground, particularly during take-off and landing, this modified lift distribution results in a change in the pitching moment. The reduction in the magnitude of the pitching moment as the aircraft's CG nears the ground can be attributed to the ground effect causing a shift in the aerodynamic centre (AC) relative to the CG (Fig. 12a).

In the context of a BWB aircraft, where the wing and fuselage are integrated, the nose-down pitching moment usually generated by the wing's lift acting ahead of the CG is mitigated. This occurs because the altered pressure

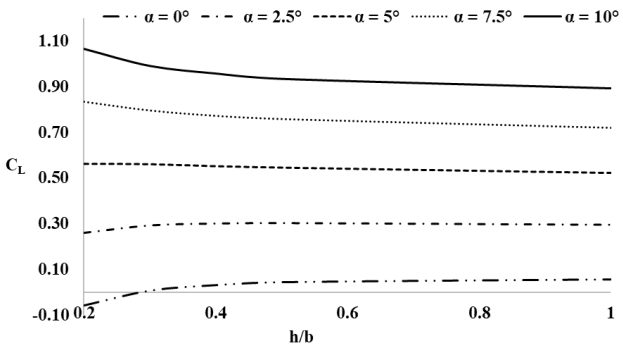

Fig. 10 C_L vs h/b at different α

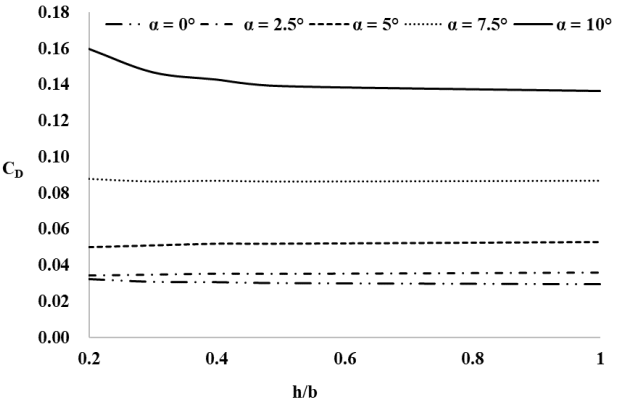

Fig. 11 C_D vs h/b at different α

distribution due to the ground effect reduces the effective leverage of the aerodynamic forces acting on the aircraft at the Fuselage Reference Line (FRL). This leads to a decrease in the nose-down tendency (How, 2004). Therefore, the phenomenon highlights the critical influence of both the ground effect on the aerodynamics of an aircraft and the imperative relationship between the C_M and the centre of gravity (CG) shown in Equation 1. The investigation also revealed a stable pitching moment within the ground effect zone, indicating minimized aerodynamic disturbances. However, as the BWB's centre of gravity (CG) neared the ground, the magnitude of the pitching moment decreased (Fig. 12b). This reduction is attributed to altered pressure distribution over the BWB's surfaces due to the ground effect, which affects lift distribution and reduces the nose-down pitching moment typically generated by the wing (Richardson, et al. 2011). This behaviour is consistent with predictions for the BWB configuration. This emphasizes the critical influence of ground effect on aircraft stability and performance, particularly during take-off, landing, and low-altitude flight. Understanding these dynamics is paramount, particularly for assessing aircraft stability and performance during low-altitude flight phases such as take-off and landing, where the proximity to the ground significantly alters aerodynamic forces and moments acting on the aircraft.

$$C_{Mcg} = (C_{Lw} + C_{Dw}\,\alpha FRL)\left(\frac{x_{cg}}{\bar{c}} - \frac{x_{ac}}{\bar{c}}\right) + C_{Ma} \quad (1)$$

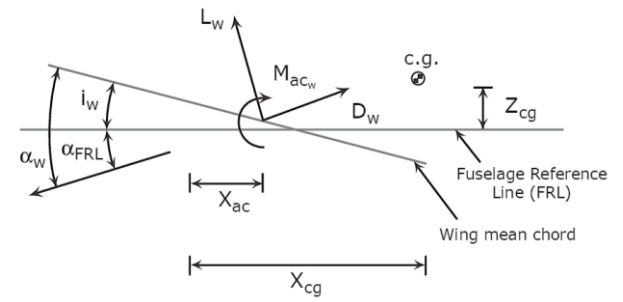

(a)

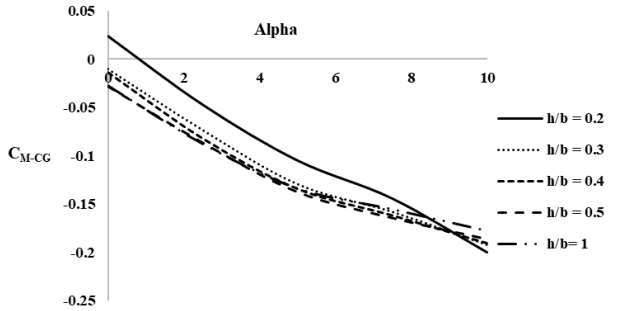

(b)

Fig. 12 (a) Schematic of $C_{M\text{-}CG}$ acting on an aircraft body (How, 2004) (b) CM-CG vs Alpha at different h/b

In analysing the aerodynamic behaviour of a BWB aircraft during ground effect interactions, the coefficient of performance (C_P), denoted in equation 2, is essential for describing the pressure differences across the wing span at various chord locations. The coefficient of pressure can be defined quantitatively by the relation:

$$C_P = (P - P_\infty) / (0.5\ \rho\ V^2) \quad (2)$$

Where P denotes the local pressure at a point on the airframe surface, P∞ represents the free-stream atmospheric pressure, ρ is the air density at sea level, and V is the free-stream velocity of the air relative to the BWB.

During initial flight conditions with an angle of attack (α) set at 0°, observation indicates a subdued C_P value, implying marginal pressure variation across the BWB's structure. This phenomenon is attributable to the alignment of the BWB with the ambient airflow, thereby reducing aerodynamic perturbations in coinciding with theoretical expectations akin to flow patterns depicted in Fig. 12a. The equation governing lift generation is mentioned in equation 3:

$$L = 0.5\ \rho\ V^2\ S\ C_L \quad (3)$$

Where S is the wing area, and C_L is the lift coefficient, implying minimal lift due to the low C_L value at α = 0° (Fig. 13a), resulting in a lower C_P at h/b = 0.2 compared to h/b = 1. As the angle of attack escalates to α = 2.5° a marked intensification in ground effect is observed, as illustrated in Fig. 13b. This pronounced ground effect can be attributed to aerodynamics principles that describe how the proximity of the BWB to the ground plane restricts the airflow beneath the wing, consequentially escalating pressure beneath the wing. This variation in pressure distribution adversely affects C_P, witnessing a discernible enhancement. This dynamic can be explained by an altered lift equation considering the ground's influence, thereby augmenting buoyancy beneath the wing. This phenomenon contributes to an increase in the C_P at h/b = 0.2.

Further advancements in the angle of attack to α = 5° and subsequently to α = 7.5°, as delineated in Figs 13c and 13d respectively, the C_P at h/b = 0.2 at α = 5° and α = 7.5° rises as demonstrate a progressive convergence in C_P values across the upper and lower surfaces of the BWB. This trend underscores an amplification in aerodynamic interference attributed to the restricted airflow, leading to increased pressure differentials. Specifically, the incidence at α = 7.5°, where a notable C_P shift is observed, particularly at dimensionless height ratios (h/b = 0.2), underscores a critical interaction threshold indicative of heightened pressure build-up beneath the BWB. Advancing to an angle of attack of α = 10° (Fig. 13e) incites a pronounced surge in C_P values, at h/b = 0.2, becomes dominant, corroborating the intensified aerodynamic interactions due to increased ground effect. The phenomenon is further exacerbated by the non-linear relationship between the angle of attack and pressure differential, as the ground effect compounds aerodynamic stresses exerted on the BWB's structure. In essence, the intricate interplay between the angle of attack, airflow dynamics, and the BWB's proximity to the ground, elucidated through quantitative analysis in Fig. 14, where a similar streamline at region 1 could be observed, which underpins the observed variations in the coefficient of pressure. This analysis provides a foundational understanding of the aerodynamic phenomena governing BWB performance near the ground surface.

Further advancements in the angle of attack to α = 5° and subsequently to α = 7.5°, as delineated in Figs 13c and 13d respectively, the C_P at h/b = 0.2 rises as demonstrate a progressive convergence in C_P values across the upper and lower surfaces of the BWB. This trend underscores an amplification in aerodynamic interference attributed to the restricted airflow, leading to increased pressure differentials. Specifically, the incidence at α = 7.5°, where a notable C_P shift is observed, particularly at dimensionless height ratios (h/b = 0.2), underscores a critical interaction threshold indicative of heightened pressure build-up beneath the BWB.

Advancing to an angle of attack of α = 10° (Fig. 13e) incites a pronounced surge in C_P values, at h/b = 0.2, becomes dominant, corroborating the intensified aerodynamic interactions due to increased ground effect. The phenomenon is further exacerbated by the non-linear relationship between the angle of attack and pressure differential, as the ground effect compounds aerodynamic stresses exerted on the BWB's structure. In essence, the intricate interplay between the angle of attack, airflow dynamics, and the BWB's proximity to the ground, elucidated through quantitative analysis in Figs 14 and 15 with ground conditions and ground-free conditions, respectively, where a velocity streamline could be observed, underpins the observed variations in the coefficient of pressure. This analysis provides a foundational

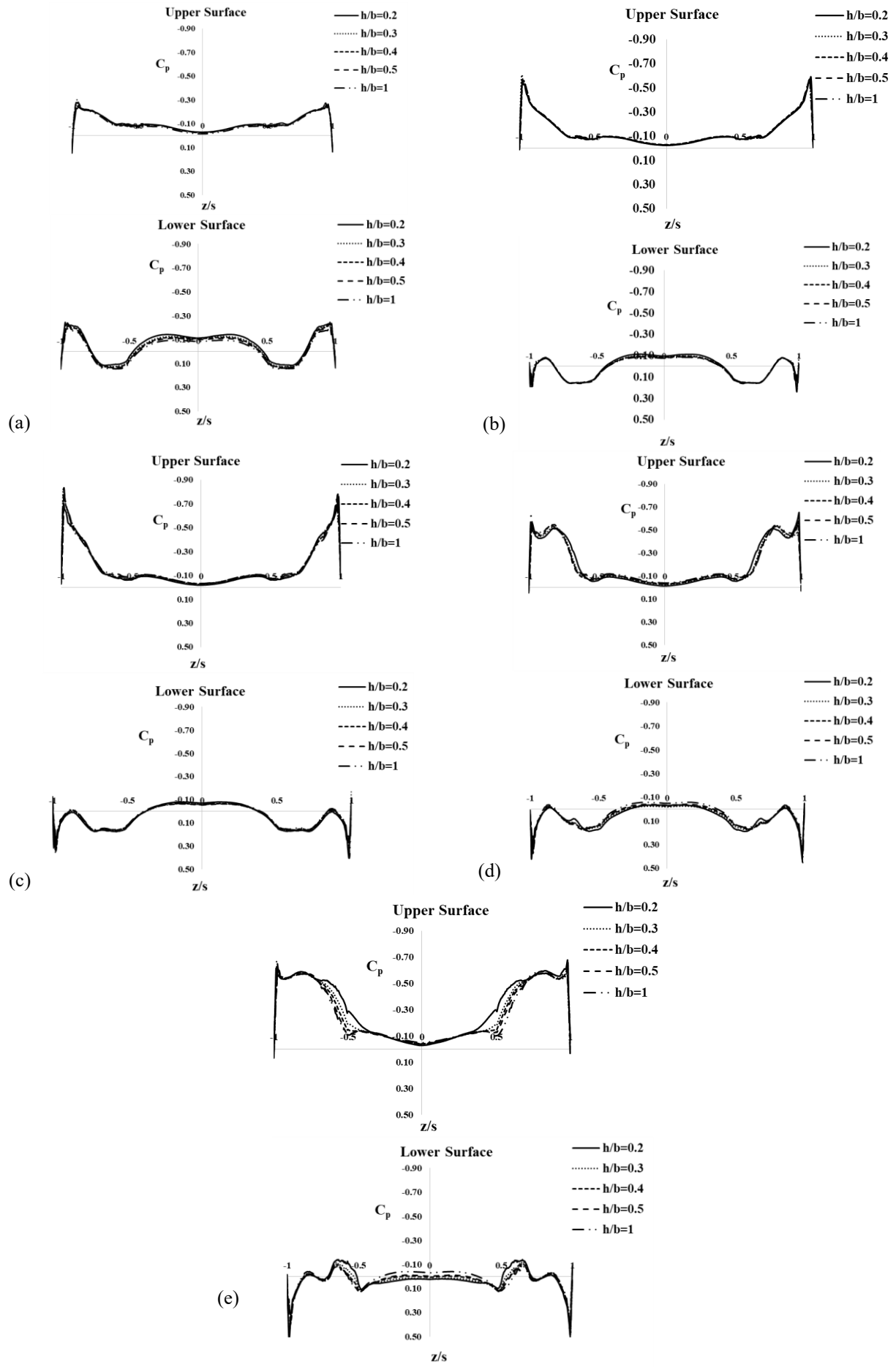

Fig. 13 C_P vs y/b at different h/b distances at x/c = 0.85 for: (a) α = 0° (b) α = 2.5° (c) α = 5° (d) α = 7.5° (e) α = 10°

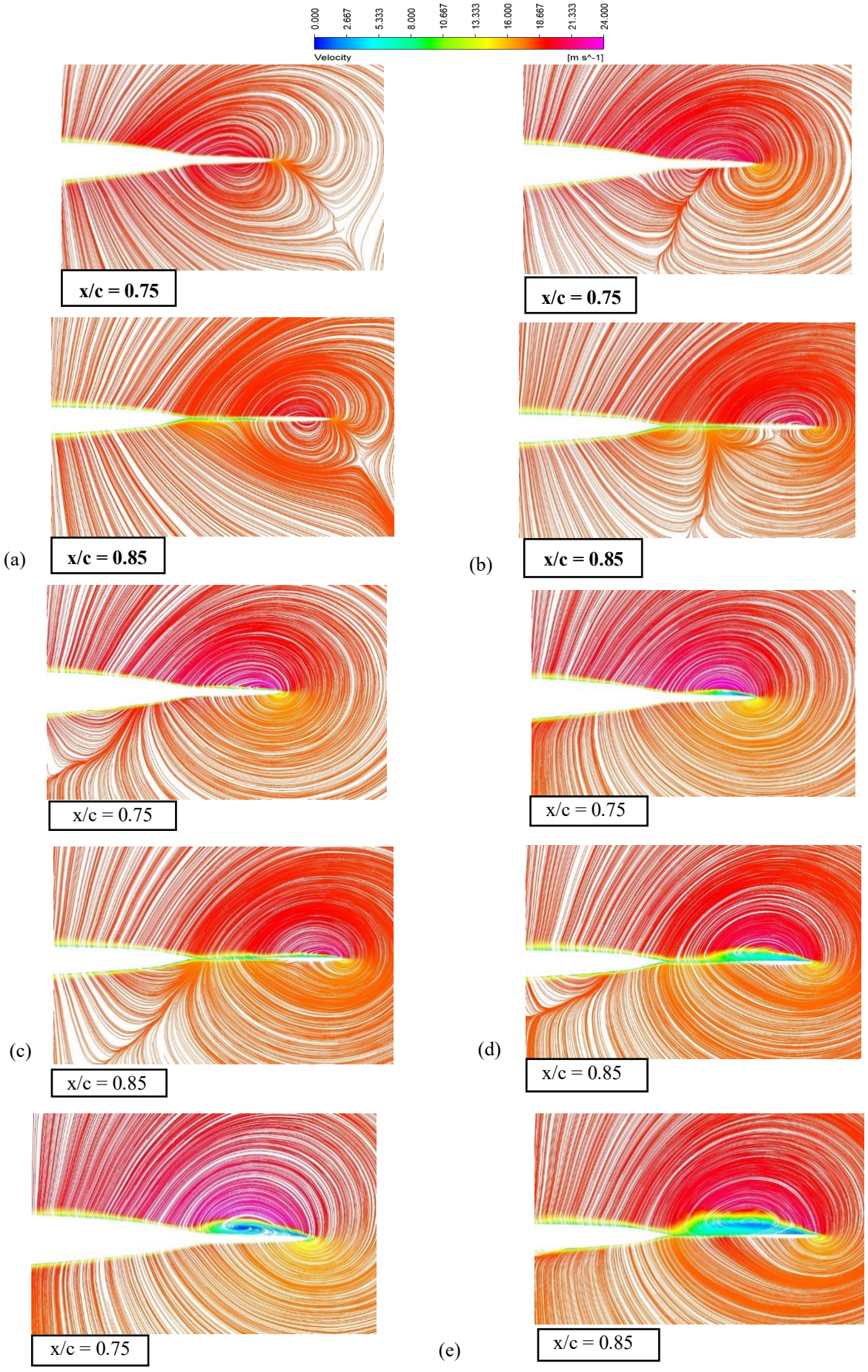

Fig. 14 Computed velocity streamlines over BWB at ground-free condition for: (a) α = 0° (b) α = 2.5° (c) α = 5° (d) α = 7.5° (e) α = 10°

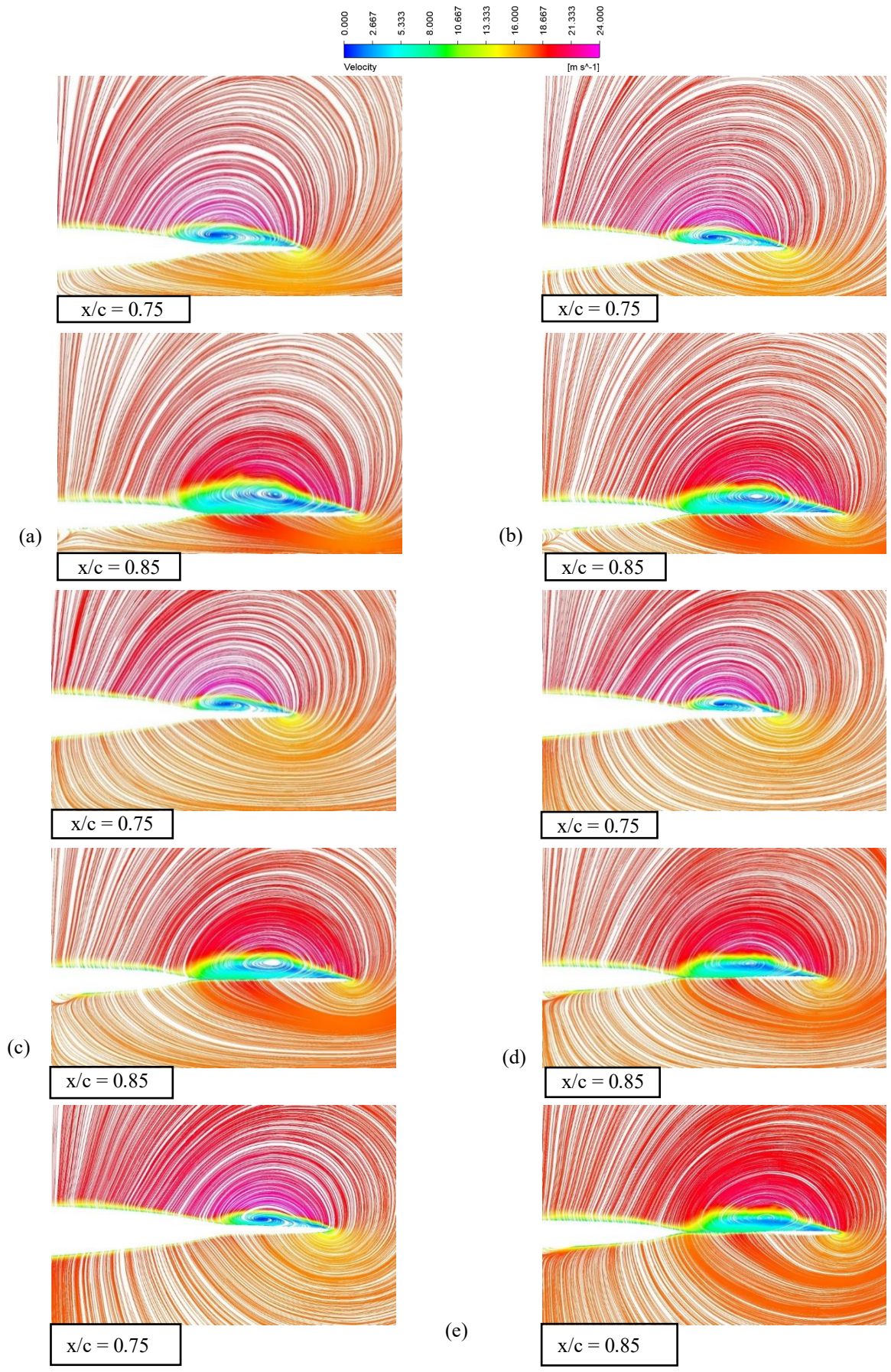

Fig. 15 Computed velocity streamlines over BWB at α = 10° condition for: (a) h/b = 0.2 (b) h/b = 0.3 (c) h/b = 0.4 (d) h/b = 0.5 (e) h/b = 1

understanding of the aerodynamic phenomena governing BWB performance near the ground-free condition. The variations observed at x/c = 0.75 and 0.85, particularly under the ground-free conditions in Fig. 14 can be attributed to the natural progression of the boundary layer and the inherent aerodynamic behaviour of the BWB's upper surface. At these chordwise locations, the local curvature of the aerofoil leads to flow acceleration, resulting in a localised reduction in static pressure as dictated by Bernoulli's principle. The velocity streamlines, as visualised in Fig. 14, reveal distinct flow phenomena, including regions of accelerated flow, pressure gradients, and potential flow separation or reattachment zones. These streamlines provide critical insights into the flow structure, particularly the formation of low-pressure zones that coincide with increased velocity, which directly governs the variations in the coefficient of pressure.

Under the ground conditions (Fig. 15), the proximity to the ground alters the free-stream flow behaviour, inducing changes in the effective angle of attack and creating a stronger adverse pressure gradient near the trailing edge. This phenomenon modifies the velocity distribution over the surface, resulting in suppressed flow separation and increased flow acceleration in certain regions due to the ground-induced compression of streamlines (Tumse et al., 2021). The comparative analysis of velocity streamlines between ground-free and ground conditions highlights the impact of the ground effect on aerodynamic forces. These observations underline the significance of understanding the interaction between flow phenomena and pressure distribution for analysing BWB designs in near-ground operations and during critical phases such as take-off and landing.

To further investigate the circulation of the velocity streamlines shown in Figs. 14 and 15, the surface integral of the particular circulation region was chosen for checking the circulation strength shown in Fig.16 and 17. This parameter plays a critical role in quantifying the lift generation and understanding the strength of the rotational flow around a lifting surface. In the context of the streamlined flow field visualized in Figs. 14 and 15, the larger magnitude of the negative circulation indicates stronger rotational flow around the aerofoil in proximity to the ground. The free-stream flow develops naturally, leading to weaker compression and reduced changes in the pressure distribution between the upper and lower surfaces. Consequently, the circulation strength decreases, as the rotational flow around the aerofoil becomes less pronounced without the ground's influence.

Streamline Density: The spacing of streamlines indicates the velocity gradient in the flow field. Where streamlines are closely packed, the flow velocity is higher, signifying stronger circulation in that region. The integral of these velocity variations around the BWB surface contributes to the circulation strength. Flow Acceleration and Vorticity: The circulation strength is directly related to the vorticity distribution in the flow. Streamlines wrapping around the leading edge and trailing edge indicate regions of high vorticity, which is a measure of the local rotational flow. Effect on Pressure Distribution: The circulation modifies the pressure

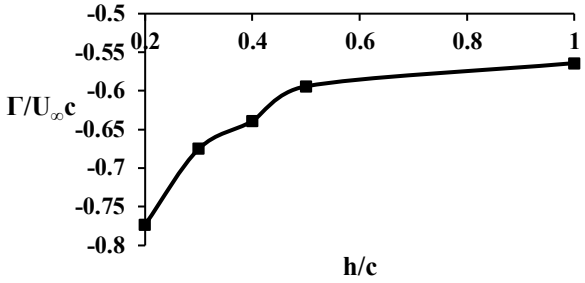

Fig. 16 Normalized computed circulation with respect to various ground height

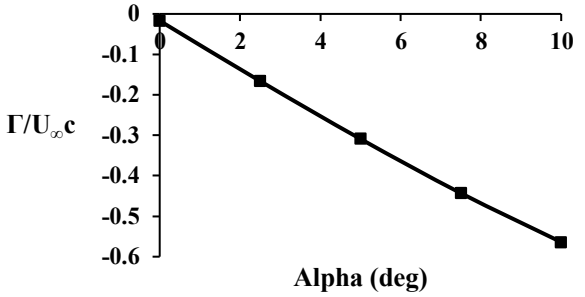

Fig. 17 Normalized computed circulation with respect to different alpha

distribution on the aerofoil, directly influencing the coefficient of pressure variations observed. Higher circulation corresponds to greater pressure differences between the upper and lower surfaces, as evidenced in the streamline visualization. Thus, Γ/(U∞ c) encapsulates the relationship between the flow field's rotational strength (as shown in Figs. 16 and 17) and the aerodynamic loading, providing a quantitative link between the streamline behavior and the aerodynamic performance metrics.

With further investigation to deep dive into flow field investigation, the pathline which are often contrasted with streamlines, and represent the direction of flow at a fixed moment in time such computational were previously studied by Mikołajczyk et al. (2023) to understand the complexity of flow around aircraft. As demonstrated in (Fig 18 a-e), keeping the BWB close to the ground and studying the phenomena at various angles of attack helped in dwelling the flow physics occurring during the ground effect vicinity. This qualitative analysis helped in finding the separating strake zones which started from the junction (region 1) at which fuselage blended with the wing.

With further advancements in ground effect quantitative studies, the relationships among C_L, C_D, and L/D as illustrated in Figures 19, 20, and 21 can be analyzed. At an angle of attack alpha of 0°, the C_L values indicate that when the aircraft is near the ground, the increased local pressure between the lower surface of the BWB and the ground causes vortices near the wing to circulate at higher velocities. This results in a slight

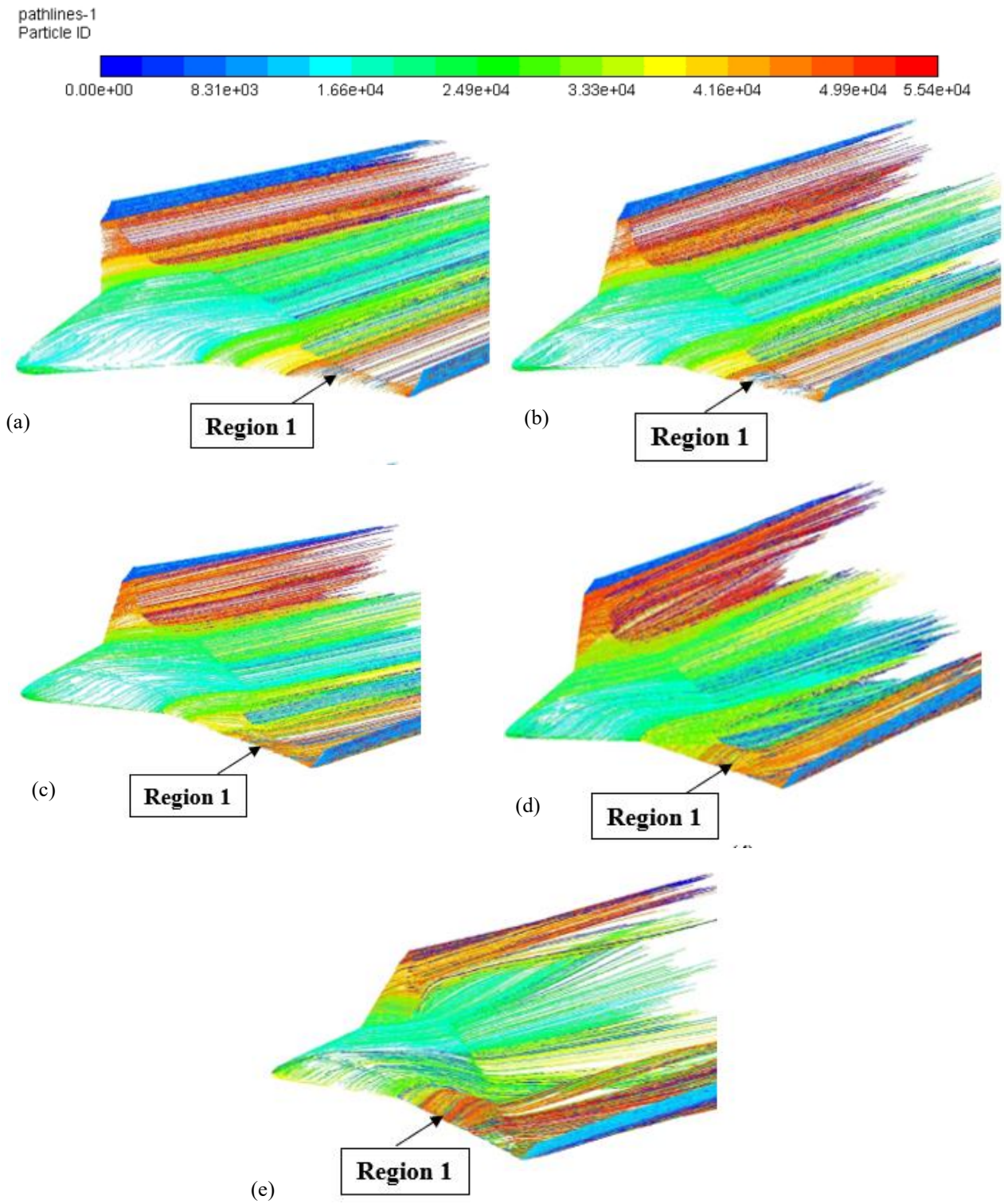

Fig. 18 Path lines at h/b = 0.2 above the BWB mid-chord for:(a) α = 0° (b) α = 2.5° (c) α = 5° (d) α = 7.5° (e) α = 10°

decrease in C_L, leading to a negative value for aerodynamic efficiency. But as soon h/b increases, the air pressure beneath the lower surface of BWB changes, causing the initial lift to the aircraft at the same α, and thus at α = 0° on increasing as ground height increases, the lift kept increasing.

This effect continues to α = 4°, and then the lift starts decreasing as the ground height increases, it is clearly visible in the figure that at higher α, the lift value decreased and even drag started increasing, which eventually proves that the air pressure at α > 4° kept on increasing which provided at additional lift when BWB was closer to the ground proximity range. The proximity to the ground amplifies these effects, leading to increased local flow velocities and pressure differentials. As α increases, the adverse pressure gradient intensifies, resulting in flow separation and increased drag. At α =

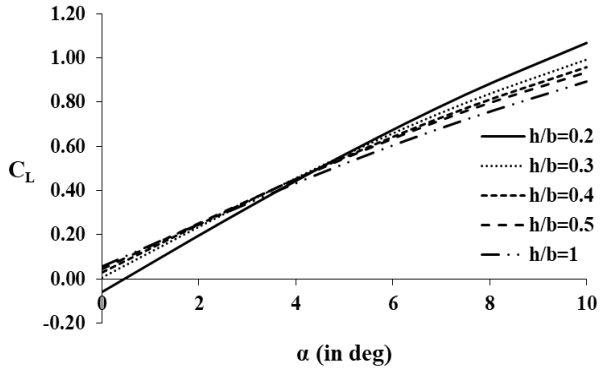

Fig. 19 Computed C_L vs α at different h/b distances

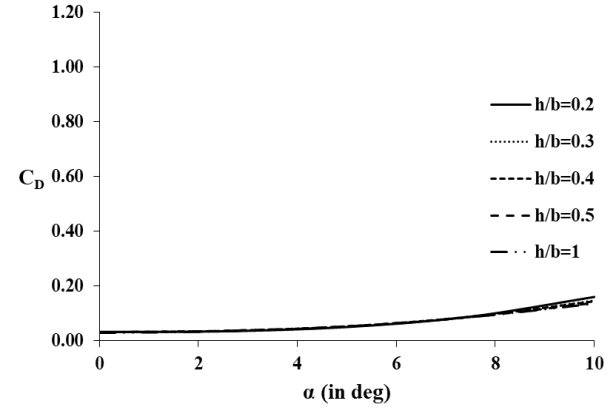

Fig. 20 Computed C_D vs α at different h/b distances

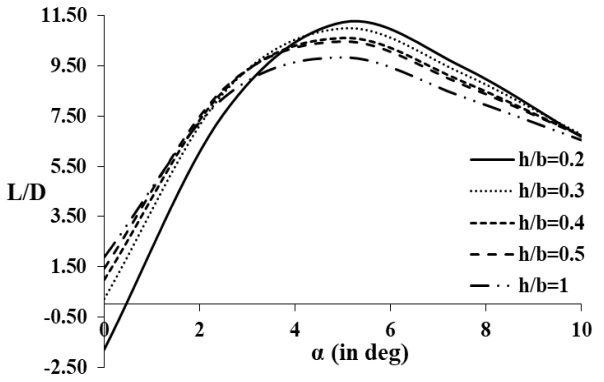

Fig. 21 Computed L/D vs α at different h/b distances

10°, the complete reversal pattern in C_L could be observed, as C_L at h/b = 0.2 had maximum lift while C_L at h/b = 1 had decreased C_L values due to an increase in adverse pressure gradient leading to flow separation with an increase in C_D near to ground i.e., h/b = 0.2 > h/b = 1.

This thorough examination of ground effect dynamics demonstrates that their proximity to the ground highly influences the aerodynamic performance of BWB aircraft. The optimal lift and drag characteristics are closely related to specific h/b ratios and angles of attack. Understanding these correlations is essential for maximizing the aerodynamic efficiency and overall performance of BWB aircraft, particularly when operating at low altitudes. These findings significantly contribute to improving the design and operational strategies for BWB configurations, ultimately leading to more efficient and effective aircraft performance.

In conjunction with these velocity observations, pressure variations were also examined to provide a more comprehensive understanding. As the ground height decreased, the pressure distribution around the wing was affected. Specifically, the pressure difference between the upper and lower surfaces was reduced, leading to less pronounced pressure differences and a more balanced pressure distribution. Near the trailing edge, the reduced downwash and improved flow attachment resulted in a more stable pressure distribution, particularly along the mid-section of the wing. It can be observed in Fig. 22 that the C_P distribution on the upper surface remains almost constant, indicating relatively steady lift generation across varying ground heights. However, the C_P distribution on the lower surface shows a "critical point" where the C_P curves coincide and then diverge as the ground effect intensifies, representing the compression of air beneath the wing as the height decreases, leading to a localized pressure spike.

Further examination in Fig. 23 reveals that at this critical point on the lower surface, the divergence of C_P on the lower surface aligns with a distinct increase in flow acceleration, indicating an impending boundary layer detachment. This detachment occurs prominently near the trailing edge, where the influence of ground proximity causes abrupt changes in pressure distribution, particularly at higher angles of attack. This finding is significant because it highlights the onset of flow instability driven by the ground effect, where reduced clearance causes a breakdown in the flow structure at the trailing zone, leading to potential flow separation. Such conditions are critical for predicting the aerodynamic behaviour of wings operating near the ground, emphasising the importance of managing pressure distribution to avoid performance degradation.

This phenomenon is particularly relevant for BWB configurations, where distributed lift surfaces make the aerodynamic response to ground effect more complex. A detailed understanding of these pressure variations can aid in refining computational models to improve predictive accuracy. Additionally, controlling flow separation through design modifications, such as optimized trailing-edge geometries or flow control mechanisms, could enhance aerodynamic efficiency in ground-effect operations.

4. CONCLUSIONS AND FUTURE WORK RECOMMENDATIONS

This research significantly contributes to analyzing the ground effect that substantially influences the aerodynamic behaviour of BWB aircraft. The study thoroughly demonstrates that the aircraft's proximity to the ground substantially modifies its lift and drag properties, notably during the crucial take-off and landing phases. The key insights derived from this investigation encompass:

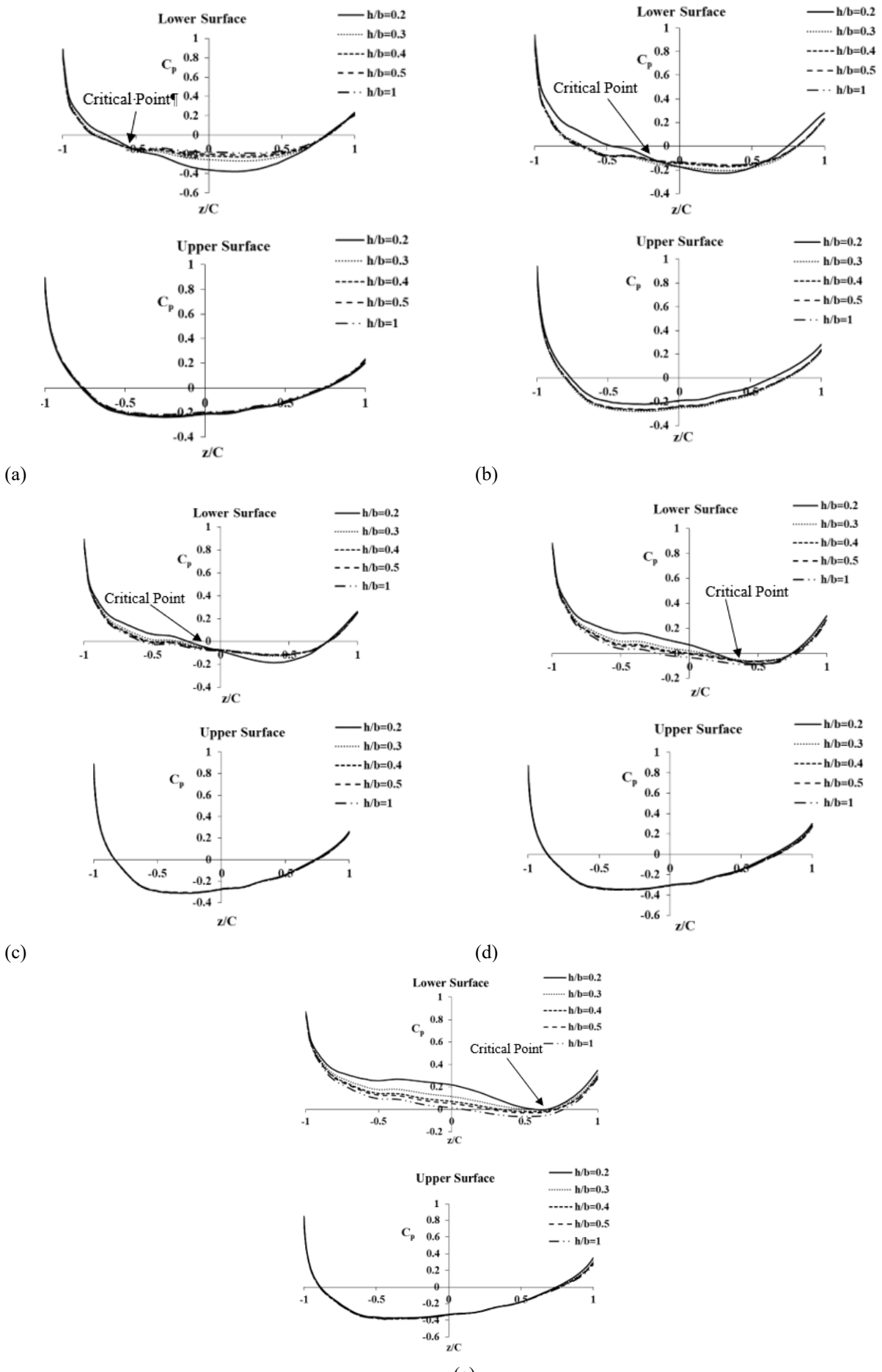

Fig. 22 C_p curve at mid-chord locations for: (a) α = 0° (b) α = 2.5° (c) α = 5° (d) α = 7.5° (e) α = 10°

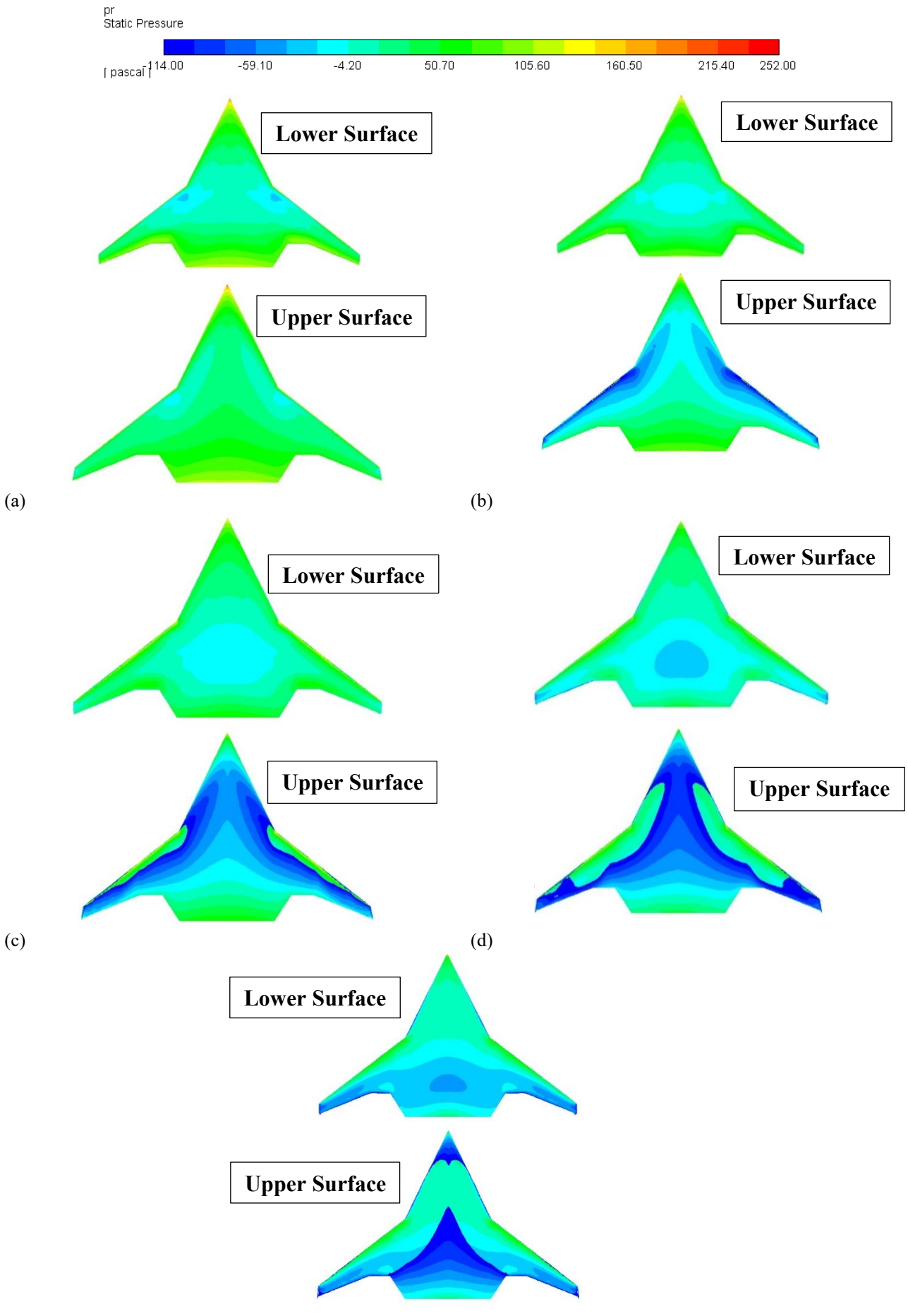

Fig. 23 Static pressure contour on lower and upper surface for h/b = 0.2 (a) α = 0° (b) α = 2.5° (c) α = 5° (d) α = 7.5° (e) α = 10°

- Lift and Drag Variations: The ground effect notably modifies the lift-to-drag ratio, with lift enhancement observed at lower angles of attack (α) and diminishes as α increases. This effect is attributed to changes in airflow patterns and pressure distribution around the aircraft, impacting both lift generation and drag.
- Pitching Moment Stability: The ground effect stabilizes the pitching moment coefficient around C.G ($C_{M\text{-}CG}$) by altering aerodynamic pressure distribution, thereby reducing the nose-down pitching tendency. This behaviour is critical for BWB aircraft stability, especially near the ground.
- Pressure Coefficient Dynamics: The coefficient of pressure (C_p) demonstrates complex interactions with angle of attack and height-to-chord ratio. The increased ground effect at lower altitudes results in higher C_P values, reflecting intensified aerodynamic interference and pressure build-up beneath the BWB.

A comprehensive grasp of these aerodynamic phenomena is crucial for optimizing BWB performance in ground effect conditions. This understanding is vital for enhancing safety and efficiency during critical phases like takeoff and landing.

These studies could identify the complex flow conditions on a typical BWB, and their complexity could enhance the approach to aerodynamic studies on such future aircraft. Overall, the research showed that the ground effect on a BWB aircraft is significant, with varying impacts on lift, drag, and pitching moment. As the aircraft flew closer to the ground, the aerodynamic characteristics changed, with the lift and pitching moment influenced by the proximity to the ground. The findings from this study provide insight into the complexities of aerodynamic conditions near the ground for future BWB aircraft designs, even for higher angles of attack.

Future research should also expand on diverse BWB designs to better understand their impact on ground effect. Advanced CFD simulations and experimental validation will refine aerodynamic models, while optimization algorithms can enhance performance. Additionally, exploring experimental techniques to capture flow phenomena during ground proximities and long-term effects will improve BWB efficiency, safety, and cost-effectiveness.

ACKNOWLEDGMENTS

The authors express their gratitude towards the Birla Institute of Technology, Mesra, for the continuous and invaluable support during the entire computational and experimental work process.

CONFLICT OF INTEREST

The authors declare that they have no conflict of interest.

AUTHORS CONTRIBUTION

Shuvendra Mohan: Research, simulations, data analysis, manuscript preparation. **Priyank Kumar:** Supervision, conceptualization, methodology, manuscript review, technical input.

REFERENCES

Ahmed, M. R., & Sharma, S. D. (2005). An investigation on the aerodynamics of a symmetrical airfoil in ground effect. *Experimental Thermal and Fluid Science, 29*(6), 633-647. https://doi.org/10.1016/j.expthermflusci.2004.09.001

Angle, G. M., O'Hara, B. M., Pertl, F. A., & Smith, J. E. (2009). Pitch stability analysis of an airfoil in ground effect. *Journal of Aircraft, 46*(3), 756-762. https://doi.org/10.2514/1.31246

Barber, T. J., Leonardi, E., & Archer, R. D. (1999). A technical note on the appropriate CFD boundary conditions for the prediction of ground effect aerodynamics. *The Aeronautical Journal, 103*(1029), 545-547. https://doi.org/10.1017/s0001924000064368

Boschetti, P. J., Neves, C. A., & González, P. J. (2022). Nonlinear aerodynamic model in dynamic ground effect at high angles of attack. *Journal of Aircraft, 59*(6), 1500-1513. https://doi.org/10.2514/1.C036721

Gebbie, D. A., Reeder, M. F., Tyler, C., Fonov, V., & Crafton, J. (2007). Lift and drag characteristics of a blended-wing body aircraft. *Journal of Aircraft, 44*(5), 1409-1421. https://doi.org/10.2514/1.22356

Gudmundsson, S. (2014). The anatomy of the airfoil. In S. Gudmundsson (Ed.), General aviation aircraft design (pp. 235–297). Butterworth-Heinemann. https://doi.org/10.1016/B978-0-12-397308-5.00008-8

How, J. P. (2004). Lecture 2: Static stability, aircraft SS (longitudinal), and wing/tail contributions, Aircraft Stability and Control (16.333) course. MIT OpenCourseWare.

Jesudasan, R., Mariani, R., & Hanifi, A. (2023). *Preliminary aerodynamic wing design optimisation for wing-in-ground Effect Aircraft.* International Conference on Evolutionary and Deterministic Methods for Design Optimization and Control with Application to Industrial and Societal Problems (EUROGEN).

Kashitani, M., Suganuma, Y., Date, H., Nakao, S., Takita, Y., & Yamaguchi, Y. (2015). *Experimental study on aerodynamic characteristics of blended-wing-body by a wake integration method*. 53rd AIAA Aerospace Sciences Meeting (p. 1228). https://doi.org/10.2514/6.2015-1228

Lee, P. H., Lan, C. E., & Muirhead, V. U. (1989). Experimental investigation of dynamic ground

effect. *Journal of Aircraft, 26*(6), 497-498. https://doi.org/10.2514/3.45793

Liebeck, R. H. (2003, July). *Blended wing body design challenges.* AIAA\ICAS International Air and Space Symposium and Exposition: The Next 100 Years, pp. 1–12. https://doi.org/10.2514/6.2003-2659

Liebeck, R. H. (2004). Design of the blended wing body subsonic transport. *Journal of Aircraft, 41*(1), 10–25. https://doi.org/10.2514/1.9084

Mikołajczyk, A., Dziubiński, A., Kurnyta-Mazurek, P., & Kachel, S. (2023). Flow around an Aircraft Model—Comparison between Hydrodynamic Tunnel Tests and Computational Fluid Dynamics Simulations. *Applied Sciences, 13*(24), 13035. https://doi.org/10.3390/app132413035

Min, B. M., Shin, S. S., Shim, H. C., & Tahk, M. J. (2008). Modeling and autopilot design of blended wing-body UAV. *International Journal of Aeronautical and Space Sciences, 9*(1), 121-128. https://doi.org/10.5139/IJASS.2008.9.1.121

Molina, J., & Zhang, X. (2011). Aerodynamics of a heaving airfoil in ground effect. *AIAA Journal, 49*(6), 1168-1179. https://doi.org/10.2514/1.J050369

Qin, N., Vavalle, A., Le Moigne, A., Laban, M., Hackett, K., & Weinerfelt, P. (2004). Aerodynamic considerations of blended wing body aircraft. *Progress in Aerospace Sciences, 40*(6), 321-343. https://doi.org/10.1016/j.paerosci.2004.08.001

Qu, Q., Wang, W., Liu, P., & Agarwal, R. K. (2015a). Airfoil aerodynamics in ground effect for wide range of angles of attack. *AIAA Journal, 53*(4), 1048-1061. https://doi.org/10.2514/1.J053366

Qu, Q., Lu, Z., Guo, H., Liu, P., & Agarwal, R. K. (2015b). Numerical investigation of the aerodynamics of a delta wing in ground effect. *Journal of Aircraft, 52*(1), 329-340. https://doi.org/10.2514/1.C032735

Richardson, T. S., Beaverstock, C., Isikveren, A., Meheri, A., Badcock, K., & Da Ronch, A. (2011). Analysis of the Boeing 747-100 using CEASIOM. *Progress in Aerospace Sciences, 47*(8), 660-673. https://doi.org/10.1016/j.paerosci.2011.08.009

Rozhdestvensky, K. V. (2006). Wing-in-ground effect vehicles. *Progress in Aerospace Sciences, 42*(3), 211-283. https://doi.org/10.1016/j.paerosci.2006.10.001

Schweikhard, W. (1967). A method for in-flight measurement of ground effect on fixed-wing aircraft. *Journal of Aircraft, 4*(2), 101-104. https://doi.org/10.2514/3.43804

Spalart, P., & Allmaras, S. (1992). *A one-equation turbulence model for aerodynamic flows.* 30th Aerospace Sciences Meeting And Exhibit (p. 439). https://doi.org/10.2514/6.1992-439

Tumse, S., Tasci, M. O., Karasu, I., & Sahin, B. (2021). Effect of ground on flow characteristics and aerodynamic performance of a non-slender delta wing. *Aerospace Science and Technology, 110*, 106475. https://doi.org/10.1016/j.ast.2020.106475

Widiawaty, C. D., Siswantara, A. I., Budiyanto, M. A., Andira, M. A., Adanta, D., Syafe'i, M. H. G., & Rizianiza, I. (2024). Analysis of mesh resolution effect to numerical result of CFD-ROM: Turbulent flow in stationary parallel plate. *CFD Letters, 16*(8), 1-17. https://doi.org/10.37934/cfdl.16.8.117

Yamada, T., Taguchi, M., Duong, N. T., Kashitani, M., Kusunose, K., & Takita, Y. (2019). *Wake measurements on blended wing body with gurney flaps in low speed flows.* AIAA Scitech 2019 Forum (p. 1617). https://doi.org/10.2514/6.2019-1617

Zhang, X., & Zerihan, J. (2003). Off-surface aerodynamic measurements of a wing in ground effect. *Journal of Aircraft, 40*(4), 716-725. https://doi.org/10.2514/2.3150